Q. J. R. Meteorol. Soc. (2002), **128**, pp. 797–817

The 7.7-year North Atlantic Oscillation

By E. D. DA COSTA* and A. COLIN DE VERDIERE
Laboratoire de Physique des Oceans, France

(Received 28 July 2000; revised 17 October 2001)

SUMMARY

We present a statistical method, the extended canonical correlation analysis, to extract intermittent propagative coupled oscillations. We have applied this technique to a 136-year-long North Atlantic sea-level-pressure and sea-surface-temperature dataset. Nine ocean–atmosphere coupled oscillations with periods between 2.3 and 18 years were found. The 7.7 y period oscillation is presented in some detail and its links with the North Atlantic Oscillation are discussed.

KEYWORDS: Correlation Coupling NAO

1. INTRODUCTION

The main focus of this paper is the periodic low-frequency coupling between the ocean and the atmosphere in the North Atlantic region. If periodic coupled oscillations explained a large amount of variance, this would be a very important step towards improving long-term weather forecasting, but even if not, such study may be of help in understanding the interaction between the ocean and the atmosphere.

Suppose that a swinging pendulum in a resistive medium such as a viscous fluid (where the damping is proportional to velocity) receives a series of random impulses acting as a driving force. It is well known that the swinging can be well represented by a linear second-order differential equation, deduced from Newton's principles, describing the motion by a deterministic sequence of causes and effects. In discrete time, the natural analogue of the linear second-order differential equation with a random driving force is a linear second-order difference equation with a random process replacing the driving force, i.e. a second-order autoregressive statistical model (e.g. Priestley 1992, p. 131). In these circumstances, a statistical description based on such a model should be statistically indistinguishable from the real data series for the deterministic pendulum excited by random impulses. Physically one may expect that the free oscillation of the pendulum which contains the pendulum physics may be extracted from a real data series of the random forced pendulum. Indeed, Priestley (1992, p. 129) has shown that one can retrieve the oscillatory behaviour of the pendulum by the analysis of the autocorrelation function of the data (although this behaviour could explain only a very small part of the variance of the actual data series). It is this approach that we are using in this work: we have assumed that the complexity of the system requires the use of statistical analysis to identify deterministic relations that are hidden in a multitude of spatial and temporal scales.

The statistical method we have introduced to extract coupled oscillations, the extended canonical correlation analysis (ECCA), explores the lag correlations between sea-level pressure (SLP) and sea surface temperature (SST) in a systematic and complete way which generalizes the techniques of Sutton and Allen (1997). We hope the statistically extracted coupled oscillations can illuminate the way ocean and atmosphere are coupled in the North Atlantic region. This can be seen as contributing to the solution of the following recurrent questions concerning the North Atlantic region: Are there preferred periods of coupled oscillations on interannual and decadal time-scales? Are they

* Corresponding author: Laboratoire de Physique des Oceans (UBO/UFR), 6 avenue Le Gorgeu, BP 809, 29285 BREST Cedex, France. e-mail: da-costa@univ-brest.fr

TABLE 1. PERIODS OF NORTH ATLANTIC OSCILLATIONS FOUNDS IN RECENT WORKS

Study	NAO period (y)											Data series
Black *et al.* (1997)	–	–	–	3.0	–	–	–	–	–	–	–	AAM (one channel) (1963–1997)
Loewe and Koslowski (1998)	–	2.3	–	–	–	–	5.8	7.8	–	–	17.9	AAIC (one channel) (1879–1992)
Melice and Roucou (1998)	–	–	–	–	–	4.2	–	–	–	12.8	–	Gridded SST (1945–1994)
Mann and Park (1996)	–	–	–	–	–	–	–	–	10.5	–	17.0	Gridded SST and SLP (1899–1993)
Moron *et al.* (1998)	2.1	2.4	–	–	–	–	–	7.5	–	12.8	–	Gridded SST (1901–1994)
Sutton and Allen (1997)	–	–	–	–	–	–	–	–	–	13.0	–	Gridded SST (1945–1989)
Tourre *et al.* (1999)	2.2	–	2.7	–	3.5	4.4	–	–	11.4	–	–	Gridded SST and SLP (1856–1991)

stationary or propagative modes? Are these modes truly coupled ocean–atmosphere modes, or do they originate from internal instabilities in either fluid? Concerning the first question, numerous analyses have identified some preferred time-scales (see Table 1). The question of propagation of SST patterns at a decadal time-scale was taken up by Hansen and Bezdeck (1996) who showed propagating patterns of SST anomalies over the Gulf Stream and the North Atlantic current regions. This propagation was further analysed by Sutton and Allen (1997) who showed that positive SST anomalies in the storm formation region near Cape Hatteras were associated with the positive phase of the North Atlantic Oscillation (NAO) dipole further north. Concerning the third question, numerous modelling studies (Weaver and Sarachik 1991; Chen and Ghil 1995; Huck *et al.* 1999) have shown that internal oceanic oscillations emerge spontaneously when an ocean model is forced by fixed buoyancy flux or coupled to a simple atmosphere in energy balance.

Using ECCA, we have detected several propagative and non-propagative periodic coupled anomalies. They include among others the oscillation described by Sutton and Allen (1997), and those reported by Tourre *et al.* (1999), but our purpose here is not to document all solutions obtained. Instead, our analysis focuses on the 7.7 y period oscillation. The atmospheric patterns of the 7.7 y oscillation corresponds nearly to the first empirical orthogonal function (EOF) pattern of the SLP anomalies. Similarly the most intense phases of the oceanic part of the 7.7 y oscillation are very nearly the same as the first EOF pattern of the SST anomalies. The first SLP and SST EOFs are frequently interpreted as representing the NAO. Even if these similarities between the 7.7 y oscillation and the EOFs provide nothing more than an indication of a possible link between the 7.7 y wave and the NAO, this is our principal reason for choosing this oscillation among the set of oscillations extracted from data by the ECCA technique.

This article is organized as follows: section 2 provides a short description of the dataset used in this paper. Section 3 provides a detailed discussion of the ECCA technique. Section 4 discusses the robustness and the sensitivity of the 7.7 y oscillation to the variation of the ECCA parameters, as well as its statistical significance. Those readers interested in the results of the statistical analysis may turn directly to section 5 in which the 7.7 y period wave is presented and the significance of its amplitude is discussed, considering that the typical measurement accuracy is rather less than the amplitude of the oscillation. In section 6 a very preliminary discussion of some physical

aspects of this oscillation is presented. Section 7 summarizes and concludes this paper. The notation used in section 3 is defined in the appendix.

2. Data

We use the 136 y SLP and SST reconstructed dataset of Kaplan *et al.* (1998a,b) to study propagative, coupled, intermittent, low-frequency oscillations. The main advantage of using this dataset, other than its exceptional duration, is the possibility of making comparisons with Tourre *et al.* (1999) who have used it with similar objectives. The data are available on a $5^\circ \times 5^\circ$ grid for the SST and a $4^\circ \times 4^\circ$ grid for the SLP as monthly averaged values obtained by optimal estimation (Kaplan *et al.* 1998a,b) from, respectively, the Met Office Global Ocean Surface Temperature Atlas (for SST and the Comprehensive Ocean–Atmosphere Data Set for SLP. This estimation fills gaps, corrects sampling errors and produces spatially and temporally coherent datasets.

From this global SST and SLP dataset, we extract a region (10°N–70°N, 100°W–8°E) which approximately coincides with the North Atlantic. The variance of the SST and SLP time series are standardized at each grid point. The anomalies and the standard deviations are derived from the long-term average at each point. The annual and the intra-annual periods of variability are filtered out at each point by an annual time running mean sub-sampled every three months.

3. Methodology

The heart of the statistical technique used in this study is a variant of the canonical correlation analysis (CCA) proposed by Barnett and Preisendorfer (1987). CCA was first described by Hotelling (1936) and, as principal components analysis (PCA), is now a very common statistical method used to study the variability of a pair of random vectors. Literature contains many examples of applications of CCA, and Preisendorfer and Mobley (1988) and von Storch and Zwiers (2000) present very detailed descriptions of this method.

CCA solves the problem of finding pairs of spatial patterns, $\alpha(x)$ and $\beta(x)$, of two space–time dependent variables, $Z_1(x, t)$ and $Z_2(x, t)$, such that their time components, $U(t)$ and $V(t)$, are optimally correlated. Barnett and Preisendorfer (1987) suggested that the filtering of the data for each field by projecting it onto a subset (explaining most of the total variance) of the EOFs of that field can make the CCA less susceptible to sampling fluctuations due to short time series. Such previous reduction of spatial degrees of freedom also avoids quasi-degeneracy of auto-covariance matrices and matrix inversions in the classical CCA approach. The variables $\alpha(x)$ and $\beta(x)$, and the eigenvalues λ^2 are obtained from

$$\left[\mathbf{C}_{PC_1PC_2}\mathbf{C}_{PC_2PC_1}\right]\boldsymbol{\alpha} = \lambda^2\boldsymbol{\alpha}, \tag{1}$$

$$\left[\mathbf{C}_{PC_2PC_1}\mathbf{C}_{PC_1PC_2}\right]\boldsymbol{\beta} = \lambda^2\boldsymbol{\beta}, \tag{2}$$

and

$$U_s(t) = \sum_{k=1}^{K_1} PC_1(k, t)\boldsymbol{\alpha}_s(k), \qquad V_s(t) = \sum_{k=1}^{K_2} PC_2(k, t)\boldsymbol{\beta}_s(k), \tag{3}$$

with $s = 1, 2, \ldots, \min(K_1, K_2)$, where $\mathbf{C}_{PC_1PC_1}$ and $\mathbf{C}_{PC_2PC_2}$ are the autocorrelation matrices, $\mathbf{C}_{PC_1PC_2}$ and $\mathbf{C}_{PC_2PC_1}$ are the cross-correlation matrices and where PC_i

represents the two sets of principal components obtained by projecting Z_i onto the space defined by its leading EOFs subset.

The loading patterns are given by

$$G_s(k) = \langle PC_1(k, t), U_s(t) \rangle_t, \qquad H_s(k) = \langle PC_2(k, t), V_s(t) \rangle_t. \tag{4}$$

(a) *Extended fields*

Let $Z_i(x_i, t)$ represent the time evolution ($t = 1, 2, \ldots, N$) of two anomaly fields ($i = 1, 2$) defined at P_i locations ($x = 1, \ldots, P_i$). The anomalies are derived from time averages at each grid point and standard deviations are computed as well to standardize $Z_i(x_i, t)$ at each grid point. After this preparatory step, ECCA starts by defining the extended variable $Y_i(p_i, t)$ by

$$Y_i(p_i, t) = \begin{cases} Z_i(x_i, t), & \text{for } p_i = x_i, \\ Z_i(x_i, t+1), & \text{for } p_i = P_i + x_i, \\ \quad \vdots & \\ Z_i(x_i, t+M), & \text{for } p_i = MP_i + x_i, \end{cases} \tag{5}$$

where $t = 1, \ldots, N - M$; $x_i = 1, \ldots, P_i$; $M = W - 1$; $i = 1, 2$; $p_i = 1, \ldots, WP_i$. The new variable $Y_i(p_i, t)$ represents the time evolution of the two extended anomaly fields defined at WP_i locations. These extended variables involve concatenating W spatial fields $Z_i(x_i, t)$ from W different times so that a large spatial field containing W time-lagged fields $Y_i(x_i, t)$ results. The variable Y_i can also be expressed by a tri-dimensional array as $Y_i(w, x_i, t)$, where $w = 1, 2, \ldots, W$ and $p_i = (w - 1) \times P_i + x_i$. This procedure is similar to either that proposed by Barnett and Preisendorfer (1987) in the context of forecasting surface air temperatures by CCA or that proposed by Weare and Nasstrom (1982) in the context of the extended empirical orthogonal function (EEOF) analysis.

ECCA proceeds by making a CCA between extended variables $Y_1(p_1, t)$ and $Y_2(p_2, t)$. But as the dimensions of arrays $Y_i(p_i, t)$ are very large, making the direct application of CCA computationally impossible to carry over, we are compelled to introduce some modifications in order to progress. These alterations do not modify the method, which can be simply described as the application of the classical CCA technique to the extended fields.

(b) *Reducing matrix dimensions*

We are now facing the type of problem that Plaut and Vautard (1994) had to solve when they reformulated the EEOF method of Weare and Nasstrom (1982). In their formulation of the Multi Singular Spectrum Analysis, the problem is solved by projecting the initial data on its EOF base and continuing the analysis in a subset of the EOF space. In this way the number of variables involved in the calculations and the matrix dimensions are reduced. At the end of the analysis, one returns to the fields in physical space through reconstruction from the EOF and principal components.

We follow the strategy of Plaut and Vautard (1994) in order to reduce the dimensionality of SST and SLP datasets by first carrying out a PCA. Two sets of leading principal components, $PC_i(q_i, t)$, ($q_i = 1, 2, \ldots, Q_i$; $i = 1, 2$) are retained to proceed, where Q_1 (Q_2) is the number of leading principal components of SST (SLP) retained.

Replacing $Z_i(x_i, t)$ by $PC_i(q_i, t)$ and x_i by q_i in (5), a new set of extended variables $X_i(r_i, t)$ is obtained.

(*c*) *Extended canonical correlation analysis*

ECCA progresses by making a Barnett and Preisendorfer's CCA between extended principal-component variables $X_1(r_1, t)$ and $X_2(r_2, t)$, $r_i = 1, 2, \ldots, WQ_i$. This is done by replacing PC_i by PE_i in (1)–(4), where PE_i represents the principal components of the extended variable X_i.

This approach introduces a new parameter to be supplied, the number of PE_i retained, denoted by K_i. This is a data filter which compresses data information in fewer variables, although it can exclude potentially useful information; K_i also controls the total number of correlated pairs furnished by the analysis. We have considered $K_1 = K_2 = K \leq 80$. The other parameters to be chosen are: the number of principal components, Q_1 and Q_2, and the window length W. If we choose Q_i too small, this results in too intensive filtering of the data and the signals that we intend to study are lost. If a large Q_i is chosen, the advantages of being in EOF space are lost: the number of variables will not be reduced significantly and no efficient filtering of the data is carried out. We have chosen here $Q_1 = Q_2 = Q \leq 10$.

The parameter W determines the time-scale of the phenomena that can be studied and its value is limited by the length of the time series.

(*d*) *Performing ECCA*

The main steps to apply the ECCA technique to SLP and SST data are summarized here.

(i) Pre-filtering of the data:
  (a) Computing anomalies fields:
    - Calculate SST′ and SLP′, i.e. the monthly anomalies relative to the climatic mean (whole dataset).
    - Filter annual and intra-annual variability: calculate annual running means for SST′ and SLP′ sub-sampled every three months, i.e. SST″ and SLP″.
    - Standardize SST″ and SLP″ at each grid point.
  (b) Reducing matrices dimensions:
    - Principal-component analysis of SST″ and SLP″: compute its principal components $PC_i(q_i, t)$, eigenvectors, and eigenvalues, $(t = 1, 2, \ldots, N;\ q_i = 1, 2, \ldots, Q_i)$.
    - Keep only first $Q = Q_1 = Q_2$ eigenvectors, principal components and eigenvalues.

(ii) Extended CCA analysis:
  (a) Define a window length W.
  (b) Compute the lagged principal-components matrix $X_i(r_i, t)$ by replacing $Z_i(x_i, t)$ by $PC_i(q_i, t)$ and x_i by q_i in (5).
  (c) Compute CCA:
    - Compute the principal components of $X_i(r_i, t)$, i.e. $PE_i(k, t)$.
    - Keep only the first K leading time series of $PE_i(k, t)$.
    - Compute the canonical components $U_s(t)$ and $V_s(t)$, the eigenvalues and the loading patterns $G_k(s)$ and $H_k(s)$ $(k = 1, 2, \ldots, K)$, by replacing PC_i by PE_i in (1)–(4).

(*e*) *Search for intermittent periodic oscillations*

The starting point for finding periodic oscillations among all components U_k, V_k, $(k = 1, 2, \ldots, K)$, produced by the ECCA, is the result for univariate signals expressed

in Vautard *et al.* (1992). The authors show that whenever an oscillation is present a pair of nearly equal eigenvalues $(k, k+1)$ stands out of the eigen-elements spectrum with time components in quadrature. In practice, the criterion to identify oscillating pairs is based on the remark that time components of oscillating pairs $(U_k, V_k, U_{k+1}, V_{k+1})$, must present similar spectral characteristics, i.e. be spectrally localized around the same frequency with similar spectral amplitudes. The same criterion remains valid for the multichannel case (Plaut and Vautard 1994). In the case of the ECCA, the previously described criterion is applied in the following mode: a periodic oscillation (represented by pair $(k, k+1)$) exists if (i) the power spectra of U_k, V_k, U_{k+1} and V_{k+1} all present a dominant spectral peak close to the same value and (ii) the amplitude of these peaks are similar. To reduce arbitrariness in the definition of 'similar frequency' we have considered that x has a value similar to y if $|y - x| < \gamma x$, and have tested the sensitivity of the results to different values of γ between 0.01 and 0.1.

(*f*) *Reconstructed components—retesting oscillatory behaviour*

Having identified the J pairs $(k_j, k_j + 1)_{(j=1,\ldots,J)}$ for which the canonical components respect the criteria described in the previous section, we can reconstruct the extended principal components, $\{E_i(r_i, t)\}_j$, associated with these pairs as:

$$\{E_i(r_i, t)\}_j = \sum_{s=k_j}^{k_j+1} G_{p_i}(s) U_s(t).$$

These reconstructed extended principal components are filtered versions of the original extended principal components $X_i(p_i, t)$: they contain only information concerning the oscillation defined by pair $(k_j, k_j + 1)$. However, these E_j are shorter than the original series PC_i (their actual length is $N - W + 1$). Vautard *et al.* (1992) have shown that the best way, in the least-squares sense, to recover full-length principal components, $\{RC_i(q, t)\}_j$, from the $\{E_i(p_i, t)\}_j \equiv \{E_i(w, q, t)\}_j$ is:

$$\{RC_i(q,t)\}_j = \begin{cases} \dfrac{1}{M}\displaystyle\sum_{w=1}^{M}\{E_i(w,q,t)\}_j, & t = M, M+1, \ldots, N-M+1, \\ \dfrac{1}{t}\displaystyle\sum_{w=1}^{t}\{E_i(w,q,t)\}_j, & t = 1, 2, \ldots, M-1, \\ \dfrac{1}{N-t+1}\displaystyle\sum_{w=t-N+M}^{M}\{E_i(w,q,t)\}_j, & t = N-M+2, \ldots, N. \end{cases}$$

As one can expect, these $RC_i(q, t)$ contain only information related to periodic intermittent oscillatory behaviour, but the criteria for pair selection described in the previous section have some arbitrariness and it is possible that some (U, V) pairs pass the test although the corresponding RC components do not present truly oscillatory behaviour. In consequence, we eliminate all pairs for which $RC_i(q, t)$ do not present a main peak in the power spectra near the peak of canonical components spectra. Our experience shows that nearly 25% of pairs selected by the criterion on the (U, V) canonical components spectra are pairs that fail this last test and are eliminated.

TABLE 2. CHARACTERISTICS OF OSCILLATIONS EXTRACTED BY EXTENDED CANONICAL CORRELATION ANALYSIS FROM SEA SURFACE TEMPERATURES AND FROM SEA-LEVEL PRESSURE

Period (years)	Oceanic explained variance (%)	Atmospheric explained variance (%)	Maximum of oceanic anomaly (degC)	Maximum of atmospheric anomaly (mb)
2.3	3	4	0.06	0.28
2.6	3	4	0.07	0.32
3.0	1	1	0.02	0.06
3.4	1	1	0.02	0.08
4.4	2	2	0.05	0.19
5.6	3	4	0.06	0.31
7.7	5	6	0.11	0.45
11.5	1	1	0.02	0.07
18.0	2	2	0.06	0.17

4. ROBUSTNESS AND STATISTICAL SIGNIFICANCE OF THE 7.7 y WAVE

It is well known that changes in the statistical-analysis parameters can produce changes in the final results. Some variability is even expected and its absence could indicate some major problem with the data or the analysis procedure. For example, if we change the number of principal components Q from one to two, we expect significant changes in the periods due to the important variance contribution of the second principal component to the global data variance. However, if definite values for the period are obtained for very different values of the parameters, we consider this as indicative of the presence of robust periodic oscillations in the dataset.

In order to test the sensitivity of the periods to variations in the parameters, we have applied ECCA for different values of W (10, 30, 100, 200 and 300), Q (2, 4, 6, 8 and 10), γ (0.01, 0.04, 0.7 and 0.1) and K (10, 20, 40, 60 and 80), all adding up to about 500 experiments. The values for periods resulting from these experiments are then grouped in classes by a cluster analysis. The results shown in this paper were obtained with $Q = 4$ (about 80% of the total variance in the dataset without annual cycle), $W = 201$ (about 50 years sampled every three months), and $K = 12$. Many algorithms have been proposed for cluster analysis; however, our results are very well separated and a simple hierarchic technique which provides a dendrogram was used. The resulting dendrogram (not shown) shows that periods are grouped in nine classes centred at 2.3, 2.6, 3.0, 3.4, 4.4, 5.6, 7.7, 11.5 and 18 y. The fact that there are so many cycles deserves, however, some prior comments. Following Loewe and Koslowski (1998) 'it would be naive to suspect the various cycles to be associated with a complementary variety of generating processes. The mathematical composition of a time series by sinusoidal oscillations should not be confused with its generation in reality'. The Loewe and Koslowski (1998) spectral analysis of the NAO index suggests that the observed cycles form a sequence of harmonic oscillations with a fundamental period of 16 y. Our results agree with this view; however, it seems more appropriate in our case to consider that such a sequence of harmonic oscillations results from the harmonic decomposition of a non-sinusoidal periodic signal of about 23 y period, for which harmonics lie at 11.5, 7.7, 5.7, 4.6, 3.8, 3.3, 2.9, 2.6 and 2.3 y, which correspond remarkably well with those we have extracted, but for the 18 y period. Newell *et al.* (1989) and Ghil and Vautard (1991) suggest that the 23 y period is associated with cyclic variations of the solar magnetic field. It was not detected here due mainly to the short length of the record. The 18 y oscillation we have detected does not appear in the above harmonic sequence;

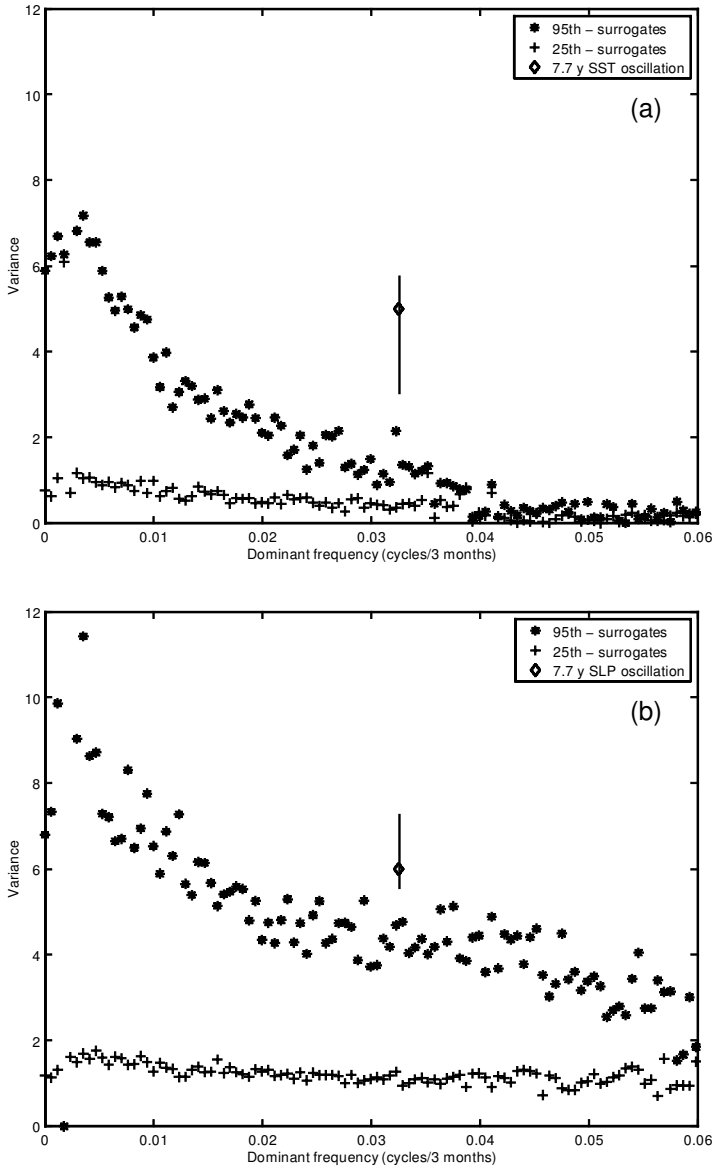

Figure 1. Test series against the AR(1) noise null hypothesis for (a) ocean and (b) atmosphere. Vertical lines over the 7.7 y oscillation variance show the distribution (between the 95th and the 5th percentiles) of the variance when we are using different parameters in the ECCA extraction of the 7.7 y oscillation from the observations.

it could originate, for example, from the lunar nodal cycle (18.6 y) as suggested by Lisitzin (1974) and Royer (1993).

If the presence of so many peaks could be explained by the harmonic sequence of the 23 y wave, this would mean that the 23 y oscillation only has physical meaning. A result somewhat in contradiction to the fact that the 7.7 y oscillation dominates the explained variance of the harmonic sequence (see Table 2; Loewe and Koslowski (1998), Fig. 2) and as such cannot be seen exclusively as a harmonic of the 23 y wave. Moreover, the 7.7 y wave presents atmospheric and oceanic patterns that are very nearly the same as the first EOF of atmosphere and ocean, frequently interpreted as the NAO patterns.

In this context the 7.7 y oscillation seems a very good candidate for studying the NAO-type coupled variability.

There is the possibility that the 7.7 y period is not statistically significant. To discuss this aspect, the significance of the frequency of the peak is obtained through a bootstrap procedure similar to that used by Tourre *et al.* (1999). The fields are randomly permuted in time one hundred times and for each permutation the ECCA is done. The ECCA have found the 7.7 y period in 90 of such permutations. Accordingly, we have estimated the statistical significance level of the 7.7 y period to 90%.

We have also tested for the significance of the 7.7 y oscillation amplitude following the approach of Allen and Robertson (1996), a Monte Carlo surrogate data testing. Our input channels are centred, pair-wise uncorrelated at lag 0, L principal components of SST and L principal components of SLP. These $2L$ independent channels have different variances and lag-1 autocorrelations. Accordingly, we test the hypothesis that $2L$ independent first-order autoregressive statistical (AR(1)) processes, individually centred, with the same variance and lag-1 autocorrelations as the input channels, could produce the same amplitude for the 7.7 y wave. The AR(1) model is computed as in Allen and Smith (1996) as

$$u_t - u_0 = \gamma^*(u_{t-1} - u_0) + \alpha^* z_t,$$

where u_0 is the process mean, z_t is a Gaussian unit-variance white noise and $\alpha^\star$ and $\gamma^\star$ are process parameters estimated from the covariances of the input channels as outlined in Allen and Smith (1996). Following the philosophy of surrogate data testing we generate a large ensemble of surrogate data segments (1000 segments) with the same length (136 y) and number of channels ($2L = 8$) as for ECCA analysis of SLP and SST data. For each surrogate segment, the ECCA procedure is done with the same values for the parameters, i.e. $W = 201$, $K = 12$. For every canonical component resulting from the ECCA analysis of the surrogate data, we compute both its variance and, via a Fourier transform, its dominant frequency. Following Allen and Robertson (1996), for each dominant frequency the distribution of variance values is computed and the 2.5th and the 97.5th percentiles are plotted in Fig. 1 against the dominant frequency associated with the corresponding canonical component. Over the same plot is shown the variance of the 7.7 y wave extracted from the SLP and SST dataset. As this variance is larger than the 97.5th percentile we conclude that there is more power in the 7.7 y oscillation than we would expect on the hypothesis that the data are nothing else than independent AR(1) processes.

5. Representing the 7.7 y period intermittent correlated oscillation

The space–time behaviour of the 7.7 y oscillation is studied by a phase-composite analysis of the reconstructed oscillations, similar to that of Plaut and Vautard (1994). Phase and amplitude indices $\theta(t)$ and $A(t)$, defining the 'instantaneous state' of the q^*th oscillation is calculated in three steps.

(i) The time derivative $\mathrm{d}\{RC_i(q^*, t)\}/\mathrm{d}t$ of the reconstructed oscillation RC_i for the time component with the largest variance q^* is calculated by finite-centred difference. Both RC_i and its time derivative are standardized by their standard deviations.

(ii) The modulus $A(t)$ and argument $\omega(t)$ of the complex number

$$I(t) = \mathrm{d}\{RC_i(q^*, t)\}/\mathrm{d}t + \mathrm{i}RC_i(q^*, t)$$

define, respectively, the instantaneous amplitude and phase of the oscillation.

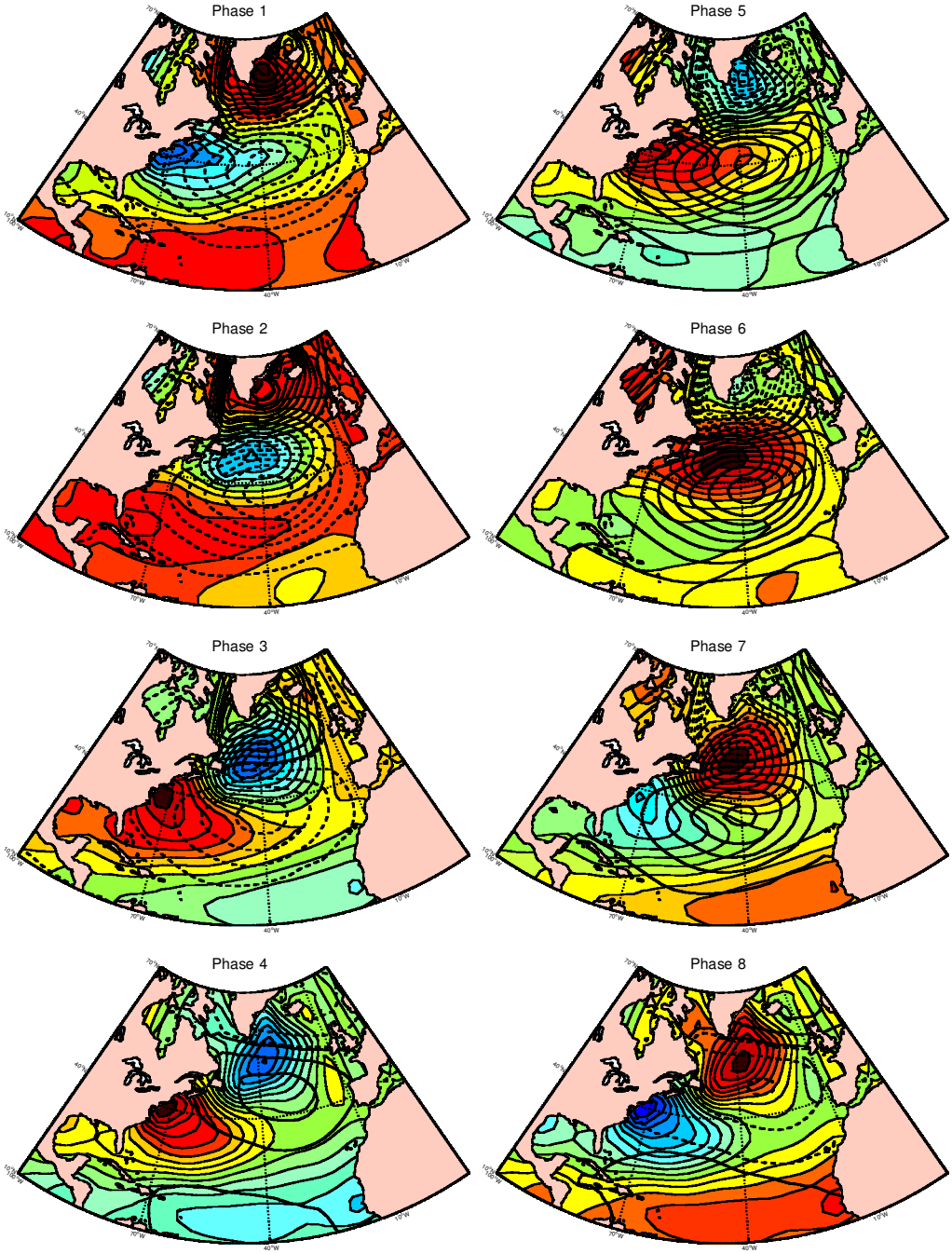

Figure 2. The life cycle of the 7.7 y intermittent periodic coupled oscillation shown through eight phases equally spaced. The contour colour fields represent the sea-surface-temperature anomalies: the red colour represents an anomaly of 0·11 degC and the blue one an anomaly of −0·11 degC. Intermediate colours are separated by −0·011 degC. For sea-level-pressure anomalies, negative contours are represented by bold dashed lines. The 0 mb line is represented by the first bold contour and the contour interval is 0.045 mb. Maximum value of the pressure anomaly is 0.45 mb.

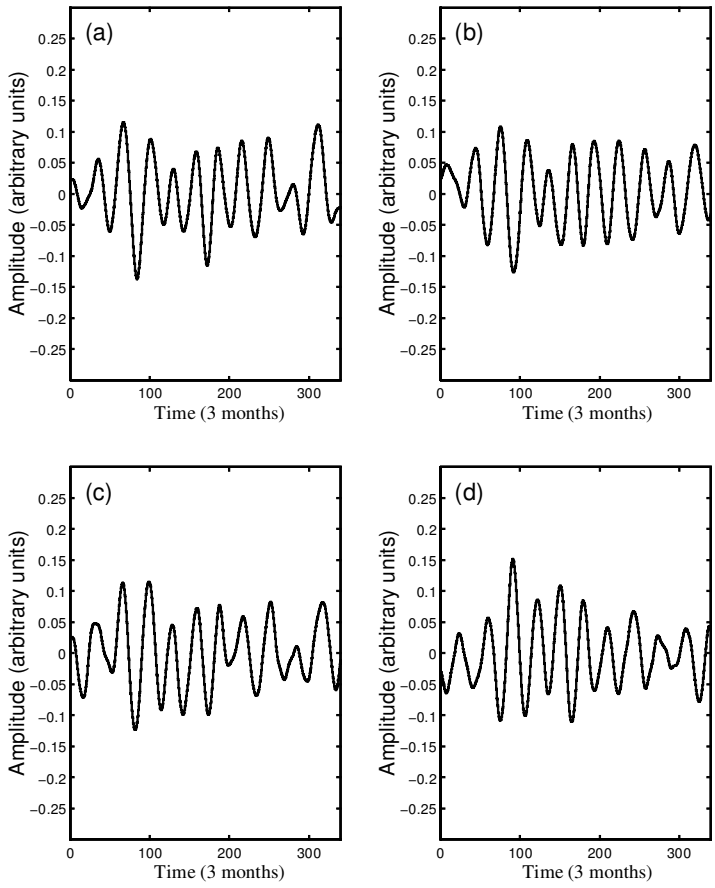

Figure 3. Extended canonical components U and V for the pair (5, 6) that contains the 7.7 y oscillation: (a) U_5, (b) U_6, (c) V_5 and (d) V_6. See text for explanation.

(iii) The mean state of the oscillation at phase θ_m can be calculated by averaging the reconstructed oscillation $RC_i(q^*, t)$ over all occurrences t when $|\theta(t) - \theta_m| < \epsilon$, where ϵ is a suitably chosen constant angular parameter (we use $\epsilon = 22{\cdot}5$) and θ_m takes the values 0, 45, 90, 135, 180, 225, 270 and 360 ($m = 1, 2, \ldots, 8$), i.e. eight phases differing by an angle of 45°.

The resulting composites values $R_i(q^*, \theta_m)$ are called phase composites and represents the 'average life cycle' of the oscillation in the leading EOFs' space. By multiplying these coefficients $R_i(q^*, \theta_m)$ by the corresponding EOFs, one obtains the average cycle in physical space.

In Fig. 2, we display the life cycle for the 7.7 y oscillation by plotting the reconstructed SLP and SST anomalies over eight phases. The amplitudes associated with these anomalies are modulated in time (see Fig. 3) and this is the reason we call them intermittent oscillations. However, this amplitude modulation is very unstable, i.e. changes in ECCA parameters produce unpredictable changes in this modulation. The intermittent character of the oscillations, although potentially very important, cannot be discussed further on the basis of our results.

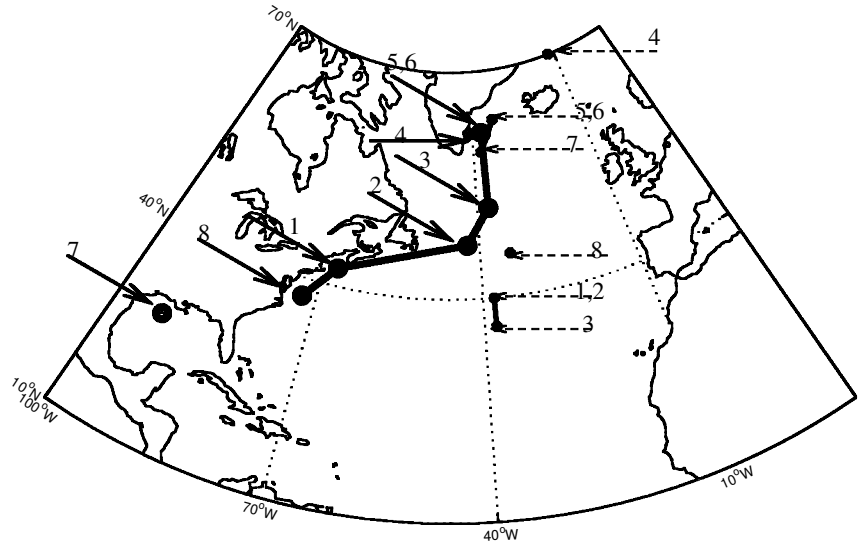

Figure 4. Trajectory of the minimum of the oceanic anomaly (thick line); positions of the atmospheric anomaly for the 7.7 y oscillation (thin line). Light (dashed) arrows points to the phase of atmospheric (ocean) anomalies according to Fig. 2 and Table 3. See Table 3 for more details on propagation speeds.

The amplitude of the SST anomaly is rather less than a typical measurement accuracy. To discuss the possibility of ECCA resolving variations of this amplitude, consider first a pure determinist signal case. In such a case, (i) and (ii) can be seen as an eigenproblem, i.e. we seek to find the eigenvalues λ and the eigenvectors $\boldsymbol{\alpha}$ and $\boldsymbol{\beta}$ of matrix $\mathbf{C}_{S1} = \mathbf{C}_{PC_1PC_2}\mathbf{C}_{PC_2PC_1}$ and $\mathbf{C}_{S2} = \mathbf{C}_{PC_2PC_1}\mathbf{C}_{PC_1PC_2}$. Considering now a series contaminated by white noise, the new matrices to be diagonalized are $\mathbf{C}_{Ri}(i = 1, 2)$ which are computed as $\mathbf{C}_{Si}$ but using the contaminated series instead. As $\mathbf{C}_{Ri}$ results from a linear filtering of the original series and since signal and noise are linearly independent, the $\mathbf{C}_{Si}$ matrix for the pure-signal case and the matrix $\mathbf{C}_{Ri}$ for the white-noise case are related by $\mathbf{C}_{Ri} = \mathbf{C}_{Si} + \mathbf{C}_{Ni}$, where $\mathbf{C}_{Ni}$ accounts for the contribution of the white noise to the final covariance matrix. However, $\mathbf{C}_{Ni}$ can be written as $\Omega\mathbf{I}$ where $\mathbf{I}$ is the identity matrix and Ω is a constant proportional to the amplitude of the white noise. Thus, $\mathbf{C}_{Ri} = \mathbf{C}_{Si} + \Omega\mathbf{I}$. But, adding $\Omega\mathbf{I}$ to $\mathbf{C}_{Si}$ simply modifies all the eigenvalues without altering the eigenvectors. We conclude that large white-noise errors in data measurements should not modify the spatial patterns of the oscillations; the ECCA provides a raising of the signal-to-noise ratio.

Concerning the spatial patterns, the 7.7 y atmospheric oscillation exhibits the familiar NAO dipole (Hurrell and van Loon 1997). Along with this SLP pattern appears the familiar tripole of SST anomalies (e.g. Tourre *et al.* 1999). Rodwell *et al.* (1999), showed that such patterns do emerge from simple regression of the SST on the NAO index. When the NAO is most intense, Fig. 2 shows a westerly intensified, coincident in latitude, 'direct' SST dipole. The term 'direct' means a positive SST lobe off Cape Hatteras and a negative lobe off Newfoundland which are associated with the positive phase of the NAO. At the difference of the SLP, these westerly intensified SST patterns are not standing but propagate along the Gulf Stream (Fig. 4) with speeds ranging from 1 to 6 cm s^{-1} (Table 3). This confirms Sutton and Allen's (1997) analysis of that particular region.

TABLE 3. LOCATIONS OF THE MINIMUM OF THE PRESSURE AND TEMPERATURE ANOMALIES FOR THE 7.7 Y OSCILLATION

Phase index	Ocean (latitude, longitude)	Anomaly speed (ocean) (cm s^{-1})	Atmosphere (latitude, longitude)
7	(27.5, −92.5)	–	(60, −38) negative NAO
8	(37.5, −72.5)	1.2	(46, −34) change of state
1	(42.5, −67.5)	5.7	(34, −38) positive NAO
2	(47.5, −42.5)	5.7	(36, −38) positive NAO
3	(52.5, −37.5)	0.9	(36, −38) positive NAO
4	(52.5, −37.5)	1.1	(70, −12) change of state
5	(62.5, −37.5)	1.2	(64, −34) negative NAO
6	(62.5, −42.5)	–	(64, −34) negative NAO
7	(27.5, −92.5)	–	(60, −38) negative NAO
8	(37.5, −72.5)	1.2	(44, −34) change of state
1	(42.5, −67.5)	5.7	(34, −38) positive NAO

What the present analysis provides is the timing between the position in latitude of the SST dipole and the NAO sign reversal. Indeed it is when the cold (warm) lobe of the SST dipole crosses the 48°N latitude of Newfoundland that the NAO reverses to positive (negative) values (see phase transition 3–4 and 7–8 in Fig. 2).

There is a further SST lobe at southern latitudes (20°N) of the same sign as the one off Newfoundland, but not as strong. It originates on the eastern side, propagates westward across the basin and reaches the Gulf of Mexico in about half a period. It hugs the western coast and intensifies markedly to become the central lobe of the SST tripole.

6. PRELIMINARY DISCUSSION OF THE PHYSICAL MECHANISMS

The observed relationship between SLP and SST fields over the 7.7 y period offers guidelines for discussing the dynamical forcings that allow the coupled system to oscillate. The first assumption to try is that this oscillation occurs independently from the rest of the signal and that wave–wave and wave–noise interactions are negligible. We show in what follows that the wind system associated with the anomalous SLP drives an oceanic SST field that has some features in common with the observations but only along the southern branch of the subtropical gyre (20°N). Such a forcing direction is suggested by the model results of Latif and Barnett (1994) for the Pacific and those of Grözner *et al.* (1998) for the Atlantic. These atmospherically forced SST anomalies are then fed into the Gulf Stream pipe and advected to the north-east. When they cross the latitude of the zero wind stress curl, the reversal of the NAO SLP dipole confirms that this area off Newfoundland is a key location for the atmospheric response to the underlying SSTs.

(*a*) *The subtropical gyre region*

We examine in some details the consequences of having the atmosphere driving the upper ocean mechanically in the subtropical gyre. To do so, we calculate the response of the upper ocean to the Ekman pumping associated with the anomalous SLP fields. At scales large compared to the Rossby radius of deformation, neglecting the advection of relative vorticity so that only long non-dispersive waves are allowed is well justified. The problem at hand is similar to that examined by Anderson and Gill (1975).

The oceanic model is a one-and-a-half layer, midlatitude, quasi-geostrophic model meant to represent the motions of the upper thermocline. It is implicitly assumed that mean and anomalies are intensified there.

The vorticity equation for the stream-function anomalies ψ , taken as linear perturbations of a predominantly zonal-mean flow can be written as:

$$\frac{\partial \psi}{\partial t} + c\frac{\partial \psi}{\partial x} = -\lambda_R^2 F. \tag{6}$$

This is the traditional long-wave equation used to describe the large-scale adjustment of the gyre to forcing through the westward propagation of the Rossby waves, where c is the phase speed, λ_R is the Rossby radius of deformation and F the forcing.

Our problem is similar to Anderson and Gill's spin-up problem, but here c is dependent upon the circulation of the gyre. To obtain the appropriate speed which is the only external parameter, we decided to rely on the study of Chelton and Schlax (1996) who have observed the westward propagation of Topex-Poseidon height signals up to 35°N in the North Atlantic. There is considerable discussion in the literature giving a proper framework to these observations which we do not want to go into. We simply make the hypothesis that such observations of westward propagations (Fig. 5(a)) are also relevant at decadal periods. The forcing F is $f w_e/h$, where the Ekman pumping w_e relates to SLP as

$$w_e = \frac{1}{\rho_0 f^2} C_D |U_T| \nabla^2(\mathrm{SLP}), \tag{7}$$

where ρ_0 is a typical value of the sea-water density, f is Coriolis parameter, C_D is the drag coefficient and $|U_T|$ is a typical turbulent wind velocity which appears when the surface drag is linearized. The forcing F can then be represented by the real part of $F_0 \sin(k_0 x) \sin(l_0 y) e^{i\omega t}$, with $k_0 = \pi/a$, $l_0 = \pi/b$, where a and b represent the zonal width of the basin and the meridional wavelength of the atmospheric forcing, respectively, mimicking the standing pattern of the NAO, maximum over the central part of the gyre and vanishing at boundaries ($x = 0$ and a and $y = 0$ and b, respectively). We will link in a simple way ψ in (6) to the SST anomaly through the hydrostatic and geostrophic relation:

$$\psi = \alpha_T g h f_0 \, \mathrm{SST},$$

where α_T is the thermal expansion coefficient, f_0 is the value of f at the middle of the domain, g is the acceleration due to gravity, and h the layer thickness of the model.

The solution to (6) is a linear combination of a free wave and a forced wave that can satisfy only one boundary condition at the eastern (western) boundary if c is negative (positive). Focusing on the southern part of the subtropical gyre, we restrict the interest to the case for which c is negative. The character of the solution depends upon the value of $\gamma = \omega/(k_0|c|) = 2a/(T|c|)$, where T is the period. If this parameter is large (slow waves), the first term in (6) dominates and the response is local with ψ (SST) lagging over SLP $(-F)$ by $\pi/2$. On the contrary, when the parameter is small (fast wave), the second term in (6) dominates and we obtain a non-local Sverdrup response integrating the forcing to its east. The response is western-intensified but nearly in phase with the SLP field. For all intermediate cases of γ values, one may then expect Sverdrup (local) response respectively in the eastern (western) basin. With $a = 5000$ km, the parameter γ (Fig. 5(b)) is less than one at low latitudes (suggesting Sverdrup response) and larger at the northern limit of the subtropical gyre indicating more local response.

When the SLP is at its maximum (Ekman pumping negative) over the subtropical gyre, the SST anomaly (proportional to the stream function) is shown to be mostly in phase with the SLP in a south-eastern region spanned by the waves. The size of this region decreases with latitude because c decreases with latitude. The response adjusts

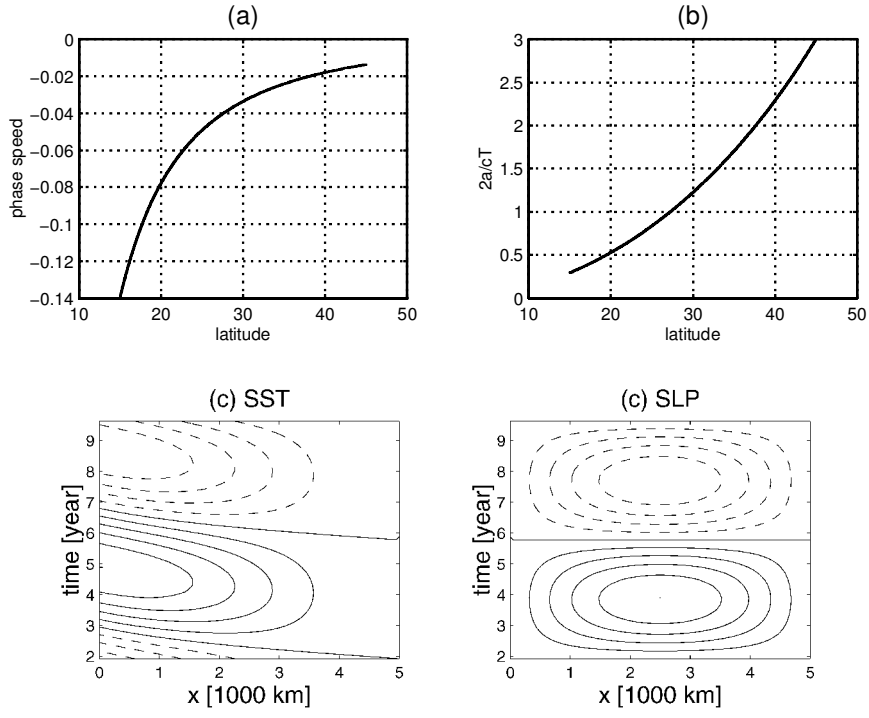

Figure 5. An analytical representation of (a) the westward phase speeds (m s^{-1}) derived from the Topex-Poseidon observations. (b) The parameter $\gamma = 2a/(cT)$ which governs the type of response of the gyre to the atmospheric forcing. (c) Characteristic (x, t) diagram showing the SST response to the SLP forcing at 20°N, positive (negative) for solid (dashed) contours. See text for explanation.

TABLE 4. AMPLITUDE OF THE OCEANIC RESPONSE AT 20°N ON THE WESTERN BOUNDARY

SLP (Pa)	w_e (m y^{-1})	ψh (10^6 m^3 s^{-1})	SST (°C)
45	5.6	0.26	4×10^{-2}

See text for explanation of symbols

quickly (slowly) to the forcing at low (high) latitudes. We suggest that the fast wave response applies to the low latitudes SST tongue (the most southerly pole of the SST anomaly in Fig. 2). Figure 5(c) shows such a solution to (6) in a characteristic (x, t) diagram at 20°N. The rapid westward propagation across the basin makes the response nearly adjusted as a Sverdrup solution across the basin. It is readily seen that the observed low (high) SST anomaly tongue at low latitudes (Fig. 1) appears to follow, with a small lag, the low (high) SLP distribution. The SST changes occur first on the eastern side of the basin as is appropriate for westward-propagating Rossby waves (Fig. 5(c)). Amplitudes of the response estimated at 20°N by the PV model have been computed in Table 4 with a thickness h of the upper layer of 400 m. The SST amplitude is within the range of observed values at such latitudes when observed SLP values are used to force the model. On the other hand, the solutions in the central and north-western part of the subtropical gyre do not compare well with the observations. Essentially the present model predicts a local response around 35°N with the SST on the western boundary

lagging over the SLP by $\pi/2$ whereas the observations show a tongue centred at Cape Hatteras which is leading the SLP by $\pi/2$. While the western intensification is predicted by the model with westward phase speeds, north of 25°N the phases suggest a different mechanism than the one embodied in (6).

(*b*) *The western boundary*

We believe that the above interior long-wave model fails at higher latitudes near the western boundary because the anomalies do not originate from the interior but from either southern latitudes or local forcing effects. The further evolution of the low-latitudes SST anomaly rationalized in section 5(a) proceeds as follows: as it enters the Gulf Stream at the latitudes of the Florida Straits, the SST tongue is advected northwards and intensifies considerably. When it reaches Cape Hatteras in its mature phase, the wind forcing that had created it in the first place at low latitudes, has now decreased to zero and reversed. The intensification of the SST from the Florida Straits to Cape Hatteras in three to four years could have several origins. One can think first of passive advection by converging streamlines in the Gulf Stream inflow region that could sharpen the anomalies locally through a purely kinematic process. A second possibility is to have the Gulf Stream itself responding to the SST anomaly. A cold (low-pressure) oceanic anomaly reaching the western boundary reduces the Gulf Stream transport geostrophically which could then lead to even lower temperatures. Such a positive feedback has been found at work in large-scale, idealized models of the oceanic circulation (Huck *et al.* 1999; Colin de Verdière and Huck 1999). A third possibility is the local effect of anomalous heat fluxes. Cayan (1992) has evaluated the relation of these heat fluxes to the SLP pattern associated with the NAO. In the NAO+ mode, Cayan finds a wide region off Cape Hatteras where the ocean loses less heat than normal, an effect caused by the increase of the southerly warm, moist wind around the Azores–Bermuda high-pressure system. When the NAO+ mode is already well developed, this anomalous flux can induce a positive feedback on the large SST anomaly. However, it falls short of explaining the presence and intensification of the SST anomaly before the onset of the NAO+ that is observed here.

(*c*) *The region off Newfoundland*

The intense anomaly described above does not stop at Cape Hatteras but continues to follow the Gulf Stream path. It is when the anomaly crosses the Newfoundland basin that the NAO dipole reverses its sign (phase 3–4 and phase 7–8 in Fig. 2). This is also the region of zero wind stress curl which has special significance for the separation of the Gulf Stream from the coast. In phase 3–4, for example, the SST structure along the western coast is dipolar increasing the climatological temperature gradient in the area. Figure 2 suggests to us that in this particular region the atmosphere responds to the SST fields (phase 4–5), intensifying the westerlies in this particular case. This results geostrophically in deepening the Icelandic Low and building up the Azores High (and vice versa when the SST dipole in its opposite phase). It has been known for a long time that this area is of special significance because of the sensitivity of the atmosphere to the underlying boundary condition. However, SST anomalies have usually been imposed as monopoles in GCMs and the results show diversity (see Peng *et al.* (1997) for a review). There is a tendency in low-resolution atmospheric GCM experiments to see a baroclinic response of the atmosphere (that is low SLP downstream of a positive SST anomaly), whereas higher-resolution experiments such as Palmer *et al.* (1985) show an equivalent barotropic response (high SLP downstream of a positive SST anomaly).

This equivalent barotropic response shows up indeed in the 7.7 y period oscillation in the building up of the NAO+ or NAO− phase (see phase 4–5 and 8–1, respectively, in Fig. 2). At such times the anomalous geostrophic winds are in the right direction to produce heat advection that reinforces the SST anomaly, a positive feedback noted by Palmer and Sun (1985). Previously mentioned anomalous heat fluxes (Cayan 1992) also have the correct sign respective to the NAO and can play a similar role. In the context of the NAO, Rodwell *et al.* (1999) recently calculated the atmospheric response to observed SST from the Global sea-Ice and Sea Surface Temperature 3.0 dataset, and concluded that much of the multiannual to multidecadal variability of the winter NAO may be reconstructed from a knowledge of the North Atlantic SST. In a second experiment, the equivalent barotropic NAO dipole stands out as the response to an idealized SST tripole distribution added to the climatological field.

How this atmospheric structure emerges is a currently debated question. It is expected that the large-scale atmospheric response is strongly dependent on the storm track. The GCM analyses of Branstator (1992, 1995) show that the storm-track activity is structured by the low-frequency waves while the momentum fluxes of the transient eddies are the primary agents for maintaining the low-frequency waves. In analysis of observations, Joyce *et al.* (2000) point out a similarity to an interaction between the Gulf Stream front and the storm count off Cape Hatteras all in phase with the NAO.

7. Summary and conclusions

This article proposes a statistical method to extract coupled oscillations. This method can be seen as an application of the ideas of Weare and Nasstrom (1982) and Plaut and Vautard (1994) to the classical CCA technique. We have named it Extended CCA. The ECCA measures the coupling between two fields (e.g. SST(x, t) and SLP(x, t)) by its time correlation. To select periodic coupled patterns of SST and SLP among all those supplied by ECCA we have followed the criterion suggested by Plaut *et al.* (1994).

The ECCA technique was applied to a 136 y North Atlantic SST and SLP dataset and the oscillations of 2.3, 2.6, 3.0, 3.4, 4.4, 5.6, 7.7, 11.5 and 18.0 y period were detected. As we were searching for NAO-type variability, the similarity between the patterns of the 7.7 y oscillation and the NAO atmospheric and oceanic patterns has led us to focus on this oscillation.

Tourre *et al.* (1999) have used the same dataset with similar objectives to ours. However, the 7.7 y period was not detected by Tourre *et al.* (1999). The differences between our results and those of Tourre *et al.* (1999) are explained by the differences in the techniques of extraction of coupled patterns. Tourre *et al.* (1999) search for dominant spatio-temporal patterns of joint SST and SLP variability. The words 'dominant' and 'joint' correspond to the two main differences between the multivariate frequency domain analysis of Tourre *et al.* (1999) and ECCA. The coupling is explicitly defined in ECCA by correlation between SST and SLP, whereas no explicit measure of coupling appears in the technique of Tourre *et al.* (1999). Secondly, Tourre *et al.* (1999) search to maximize the variance of the joint modes while ECCA maximizes the correlation of coupled modes. These two methods isolate different frequencies and, in some cases, associate very different spatial patterns with the same frequency. Which of these methods is the correct one, i.e. provides the physically correct coupled modes of oscillation, is a question that cannot be answered only on purely statistical grounds. What is offered here is the hypothesis that ECCA extracts from the data statistically coupled patterns which are also candidates to help build the physics behind the NAO coupled variability.

The patterns and the type of propagation associated with the 7.7 y coupled oscillation are somewhat similar to those described by Sutton and Allen (1997), who have estimated, however, a different value for the period (12–14 y). This discrepancy leads us to believe that we are effectively in the presence of two different oscillations. As Sutton and Allen (1997) have used five-year running averages, the variance in the 7.7 y mode becomes drastically reduced and the 12 y mode emerges then as the most important, in contradiction with our results. The ECCA on the other hand, also extracts an 11.5 y oscillation (not shown) which may be closer to the one found by Sutton and Allen but of lesser variance and statistical significance, and less similar to the NAO patterns.

To discuss the physics behind the 7.7 y wave we have identified three regions with distinctive interactions, corresponding to the SST tripole anomaly, namely, the subtropical gyre, the western subpolar gyre and the Gulf Stream path. In the subtropical gyre, model studies for the Pacific by Latif and Barnett (1994) and by Grözner *et al.* (1998) for the Atlantic indicate that the decadal anomalies gyres are induced by the wind-stress-curl anomalies. We tested this idea using a simple long-wave model with limited success. It only appears to work in the southern limb of the subtropical gyres. In fact, given the rapid phase speed of the long wave and the low frequency of the wind-stress-curl forcing, the oceanic response is nearly of a Sverdrup type (which integrates the forcing from the east). When the SST is computed hydrostatically from the quasi-geostrophic pressure, the small phase lag between the forcing deduced from the SLP and the SST as well, as the amplitudes of the SST anomalies, compares favourably with observed signals.

At higher latitudes (25°N and beyond) the phase speed of the long waves are too slow and the SST model response lags the atmospheric forcing, in contrast with the observations that show a strongly western-intensified SST leading the SLP by a few years. This intensification of the SST occurs in the formation region of the 18 °C water (the subtropical mode water). At this subtropical latitude, the oceanic observed response does not appear to be the result of a forcing of the zonal wave guide but instead the result of an ocean–atmosphere interaction mechanism local to the western-boundary wave guide. Although its origin is unclear at the present time, the above phase lags suggest that the atmospheric changes follow those in the ocean at these latitudes. Joyce *et al.* (2000) have found a good correlation between the NAO index, the presence of 18 °C water at Bermuda and the Gulf Stream front all with zero lag. They note, however, that the SST leads over the buoyancy forcing in the region where the Gulf Stream leaves the coast—a result which may agree qualitatively with ours when we consider the evaporation contribution to the buoyancy forcing caused by anomalous wind circulation patterns. They point out further that the modification of the storm track linked to the displacement of the Gulf Stream front has to be taken into account as well.

Near 45°N and beyond we observe a strong sensitivity of the atmosphere: the NAO dipole reverses when the western-intensified SST anomaly crosses the latitude of the zero wind stress curl. A high (low) SLP anomaly builds up rapidly east of a high (low) SST anomaly reminiscent of the equivalent barotropic response found for instance in Palmer and Sun (1985) model study. This sensitivity supports the recent results of Rodwell *et al.* (1999) who stress the realism of the atmospheric decadal response to observed and idealized tripole SST distributions.

To summarize, the observed phase lags between SST and SLP at the 7.7 y period reveal the inadequacy of a long-wave model except for low tropical latitudes and suggest a more local ocean–atmosphere interaction near the western boundary. At these higher latitudes the interactions of the large-scale oscillation with the storm track will need to be taken into account, as suggested by Joyce *et al.* (2000).

ACKNOWLEDGEMENTS

The stay of Eduardo Damasio da Costa at Laboratoire de Physique des Oceans is funded by the Ministerio de Ciencia e Tecnologia (Portugal). This work is a contribution from UMR 6523 (Centre Nationale de la Recherche Scientifique-Institute Français de Recherche pour l'Exploitation des Mers-UBO).

APPENDIX

Notation

$\boldsymbol{\alpha}$, $\boldsymbol{\beta}$	Eigenvectors in canonical correlation analysis
λ	Eigenvalues in canonical correlation analysis
$\theta(t)$	Oscillation phase index
θ_m	Angle for which averaged oscillation is computed
ϵ	Angle in EOF space for phase averaged oscillation fields
$A(t)$	Amplitude index
$\mathbf{C}_{xy}$	Matrix of covariances between x and y
$\{E_i(r_i, t)\}_j$	Reconstructed extended PC for the jth oscillation
$G_s(k)$, $H_s(k)$	sth canonical loading patterns
i	$i = 1$ denotes SST data and $i = 2$ denotes SLP data
j	Index denoting the jth oscillation isolated by ECCA
J	Total number of periods identified by ECCA
k	k th canonical component furnished by the ECCA: $k = 1, \ldots, K$
K	Number of canonical components retained into ECCA
m	Number of phases where composite oscillations are computed
M	Number of time lags in ECCA: $M = W - 1$
N	Actual length of time series for SST and SLP datasets
p_i	Location index of points in extended fields: $(p_i = 1, \ldots, WP_i)$
P_i	Actual number of locations for SST and SLP datasets
$PC_i(q_i, t)$	Principal components of SST and SLP anomaly fields
$PE_i(k, t)$	Principal components of X_i
q^*	Index of the RC_i component with larger variance
q_i	Principal components index: $(q_i = 1, \ldots, Q_i)$
Q	Number of principal components retained for ECCA
r_i	r_ith PC inside the extended-PC variable: $(r_i = 1, \ldots, WQ_i)$
$\{RC_i(q, t)\}_j$	PC for the jth canonical component furnished by ECCA
s	Index denoting the sth canonical component furnished by ECCA
S	Total number of canonical components furnished by ECCA: $S = W \times Q$
t	Time index: $(t = 1, \ldots, N)$
$U_s(t)$, $V_s(t)$	sth canonical time components
w	wth field inside the extended field Y_i: $(w = 1, \ldots, W)$
W	Window length for ECCA
x_i	Location index of points in each field Z_i: $(x_i = 1, \ldots, P_i)$
$\langle x(t), y(t)\rangle_t$	Euclidean dot product between $x(t)$ and $y(t)$
$X_i(r_i, t)$	Extended principal components
$Y_i(p_i, t)$	SST ($i = 1$) and SLP ($i = 2$) extended anomaly fields
$Z_i(x_i, t)$	SST ($i = 1$) and SLP ($i = 2$) anomaly fields

REFERENCES

Allen, M. and Robertson, A. 1996 Distinguishing modulated oscillations from coloured noise in multivariate datasets. *Clim. Dyn.*, **12,** 775–784

Allen, M. and Smith, L. 1996 Monte Carlo SSA: Detecting irregular oscillations in the presence of colored noise. *J. Climate*, **9,** 3373–3403

Anderson, D. and Gill, A. 1975 Spin up of a stratified ocean with application to upwelling. *Deep-Sea Res.*, **22,** 583–596

Barnett, T. and Preisendorfer, R. 1987 Origins and levels of monthly and seasonal skill for United States surface air temperatures determined by CCA. *Mon. Weather Rev.*, **115,** 1825–1850

Black, X., Salstein, D. and Rosen, R. 1997 Interannual modes of variability in atmospheric angular momentum. *J. Climate*, **9,** 2834–2849

Branstator, G. 1992 The maintenance of low frequency anomalies. *J. Atmos. Sci.*, **49,** 1924–1945

1995 Organization of storm track anomalies by recurring low frequency circulation. *J. Atmos. Sci.*, **52,** 207–226

Cayan, D. 1992 Latent and sensible heat flux anomalies over the northern oceans: The connection to monthly atmospheric circulation. *J. Climate*, **4,** 354–369

Chelton, D. and Schlax, M. 1996 Global observations of oceanic Rossby waves. *Science*, **272,** 234–238

Chen, F. and Ghil., M. 1995 Interdecadal varaibility of the thermohaline ciruclation and high latitude surface fluxes. *J. Phys. Oceanogr.*, **25,** 2547–2568

Colin de Verdière, A. and Huck, T. 1999 Baroclinic instability: An Oceanic wavemaker for interdecadal variability. *J. Phys. Oceanogr.*, **29,** 893–910

Ghil, M. and Vautard, R. 1991 Interdecadal oscillations and the warming trend in global temperature time series. *Nature*, **350,** 324–327

Grözner, A., Latif, M. and Barnett, P. 1998 A decadal climate cycle in the North Atlantic Ocean as simulated by the Echo coupled GCM. *J. Climate*, **11,** 831–847

Hansen, V. and Bezdek, F. 1996 On the nature of decadal anomalies in North Atlantic sea surface temperature. *J. Geophys. Res.*, **101,** 8749–8758

Hotelling, H. 1936 Relations between two sets of variates. *Biometrika*, **28,** 321–377

Huck, T., Colin de Verdière, A. and Weaver, A. 1999 Interdecadal variability of the thermohaline circulation in box-ocean models forced by fixed surface fluxes. *J. Phys. Oceanogr.*, **29,** 865–892

Hurrell, W. and van Loon, H. 1997 Decadal variations in climate associated with the North Atlantic Oscillation. *Clim. Change*, **36,** 301–326

Joyce, T., Deser, C. and Spall, M. 2000 On the relation between decadal variability of subtropical mode water and the North Atlantic Oscillation. *J. Climate*, **13,** 2550–2569

Kaplan, A., Cane, M., Kushnir, Y., Clement, A., Blumenthal, M. and Rajagopalan, B. 1998a Analyses of global sea surface temperature 1856–1991. *J. Geophys. Res.*, **102,** 27835–27860

Kaplan A., Cane, M. and Kushnir, Y. 1998b Reduced space optimal interpolation of historical sea level pressure: 1854–1992. *J. Geophys. Res.*, **103,** 18567–18589

Latif, M. and Barnett, T. 1994 Causes of decadal variability over the North Pacific and North America. *Science*, **226,** 634–637

Loewe, P. and Koslowski, G. 1998 The western Baltic Sea ice season in terms of a mass-related verity index 1879–1992. *Tellus*, **50A,** 219–241

Lisitzin, E. 1974 *Sea level changes*. Elsevier Scientific Publishing Company, Amsterdam

Mann, E. and Park, J. 1996 Joint spatiotemporal modes of surface temperature and sea level pressure variability in the northern hemisphere during the last century. *J. Climate*, **9,** 2137–2162

Melice, L. and Roucou, P. 1998 Decadal time scale variability recorded in the Quelccaya summit ice core $\delta^{18}O$ isotopic ratio series and its relation with sea surface temperature. *Clim. Dyn.*, **14,** 117–132

Moron, V., Vautard, R. and Ghil, M. 1998 Trends, interdecadal and interannual oscillations in global sea surface temperatures. *Clim. Dyn.*, **14,** 545–569

Newell, N., Newell, R., Hsiung, J. and Zhongxiang, W. 1989 Global marine temperature variation and the solar magnetic cycle. *Geophys. Res. Lett.*, **16,** 311–314

Palmer, T. and Sun, Z. 1985 A modelling and observational study of the relationship between sea surface temperature in the north-west Atlantic and atmospheric general circulation. *Q. J. R. Meteorol. Soc.*, **111,** 974–975

Plaut, G. and Vautard, R. 1994 Spells of low-frequency oscillations and the weather regimes in the northern hemisphere. *J. Atmos. Sci.*, **51,** 210–236

Peng, S., Robinson, W. and Hoerling, M. 1997 The modeled atmospheric response to midlatitude SST anomalies and its dependence on background circulation states. *J. Climate*, **10,** 971–987

Preisendorfer, W. and Mobley, C. 1988 *Principal component analysis in meteorology and oceanography*. Ed. C. Mobley. Elsevier, Amsterdam

Priestley, M. 1992 *Spectral analysis and time series*. Academic Press, New York

Rodwell, M., Rowell, D. and Folland, C. 1999 Oceanic forcing of the wintertime North Atlantic Oscillation and European climate. *Nature*, **398,** 320–323

Royer, T. 1993 High latitude oceanic variability associated with the 18.6 year nodal tide. *J. Geophys. Res.*, **98,** 4639–4644

Sutton, T. and Allen, M. 1997 Decadal predictability of North Atlantic sea surface temperature and climate. *Nature*, **388,** 563–567

Tourre, M., Rajagopalan, B. and Kushnir, Y. 1999 Dominant patterns of climate variability in the Atlantic ocean region during the last 136 years. *J. Climate*, **12,** 2285–2299

Vautard, R., Yiou, P. and Ghil, M. 1992 Singular Spectrum Analysis: A toolkit for short, noisy chaotic signals. *Physica*, **58,** 95–126

von Storch, H. and Zwiers, F. 2000 *Statistical analysis in climate research*. Cambridge University Press

Weare, B. and Nasstrom, J. 1982 Examples of Extended Empirical Orthogonal Function Analyses. *Mon. Weather Rev.*, **110,** 481–485

Weaver, A. and Sarachik, E. 1991 Evidence for decadal variability in an ocean general circulation model: An advective mechanism. *Atmos.–Ocean*, **29,** 197–231